IEEE Access
Multidisciplinary | Rapid Review | Open Access Journal

Received June 14, 2021, accepted July 25, 2021, date of publication July 30, 2021, date of current version August 9, 2021.

Digital Object Identifier 10.1109/ACCESS.2021.3101214

Quantum Error Mitigation for Quantum State Tomography

SYAHRI RAMADHANI, JUNAID UR REHMAN, AND HYUNDONG SHIN, (Fellow, IEEE)
Department of Electronics and Information Convergence Engineering, Kyung Hee University, Giheung-gu, Yongin-si, Gyeonggi-do 446-701, South Korea
Corresponding author: Hyundong Shin (hshin@khu.ac.kr)

This work was supported by the National Research Foundation of Korea (NRF) Grant through the Ministry of Science and ICT (MSIT) of Korea Government under Grant 2019R1A2C2007037.

ABSTRACT Quantum state tomography (QST) is the task of statistically constructing the density matrix of an unknown quantum state by measuring its several copies. The presence of noise in the QST setup can considerably degrade the fidelity between the constructed density matrix and the actual state. We consider a noisy QST setup with depolarizing noise and attempt to mitigate the effects of noise by quantum error mitigation (QEM). We compare the performance of different QEM methods with the same resources and find that the measurement error mitigation and zero noise extrapolation provide the best performance in terms of maximizing the fidelity between the state and its density matrix.

INDEX TERMS Least square error mitigation, measurement error mitigation, neural network error mitigation, quantum depolarizing channel, quantum error mitigation, quantum state tomography, zero noise extrapolation.

I. INTRODUCTION

Quantum state tomography (QST) is an important task in quantum information processing to identify an unknown but physically available quantum state [1], [2]. The two key steps in QST are the measurement of an ensemble of identically prepared quantum systems and the reconstruction of quantum states from the measurement results. The first method developed to reconstruct a quantum state was the linear inversion introduced in [3]. However, due to the experimental noise, the reconstructed states may not be a physical one. This problem of unphysical constructed states was solved in the maximum likelihood QST [4]–[6]. Another method that additionally uses prior information regarding the quantum states is the Bayesian tomography [7]–[9]. The linear regression (LR) method was also developed to accelerate the QST process [10], [11]. Recently, machine learning methods are actively being used to improve the accuracy of QST since its robustness to noise [12]–[15].

These methods of QST rely entirely on the statistics from the state measurements. Despite the significant progress in the methods of QST, noise in the state evolution before measurement and in the measurement device itself may provide measurement statistics that are not representative of the actual state. These corrupted statistics then lead to low fidelity estimates of the actual quantum state [16], [17] and the high fidelity states cannot be reconstructed even though the copies of the unknown state are measured [18], [19].

Quantum error mitigation (QEM) is a recently proposed method that reduces errors caused by noisy quantum devices/environments. QEM methods aim to recover the ideal measurement probabilities or expectation values from the noisy ones. Many QEM methods have been developed in the past few years. For example, [20]–[23] mitigates the errors by using the Richardson's extrapolation method. This method has been experimentally implemented in [24]–[26]. Other methods of QEM include the measurement error mitigation [27], [28], QEM based on least square fitting [29], and machine learning-based QEM [30]–[33]. Since the QST can be recast as estimating the expectation values of the measurement operators over the unknown quantum state, QEM seems a viable method to mitigate the effects of noise in noisy QST.

Here, we implement the aforementioned QEM methods to mitigate the effect of noise in a QST setup affected by the depolarizing noise. We utilize the LR QST and compare the performance of measurement error mitigation (MEM), zero noise extrapolation (ZNE), least square

The associate editor coordinating the review of this manuscript and approving it for publication was Siddhartha Bhattacharyya.

error mitigation (LSEM) and neural networks-based QEM (NNEM). We perform numerical simulations to demonstrate the performance of these QEM methods in correcting the measurement errors and find the best method for reconstructing noise-free quantum states with limited resources.

Our main focus in this work is to compare the performance of different QEM schemes in a similar noisy environment and with equivalent resource utilization. To this end, we fix the noise to be of depolarizing form due to its simplicity, common occurrence in many quantum information processing tasks, and the possibility of transforming other channel models into a depolarizing channel via twirling [28]. The main contributions of this paper can be summarized as follows

1) We demonstrate the applicability of different QEM schemes for the task of QST. This applicability enables the reconstruction of high fidelity estimated quantum state in a noisy QST setting.
2) We perform the numerical experiments for different QEM schemes and compare their performances on reconstructing the density matrix of the unknown states. For a proper comparison, each QEM scheme utilizes the same amount of total resources for performing the tomography measurement and the QEM tasks. By utilizing the same amount of resources, we found that the MEM and the ZNE give the best performance among other QEM methods under study.
3) For each QEM considered in our paper, we consider different resource allocation schemes for the tomography measurement and the post-processing (QEM). In this setting, we determine the best resource allocation for each QEM-QST scheme.

The remainder of this paper is organized as follows. In Section II, we provide the basic concepts of LR QST and the aforementioned QEM schemes. The numerical simulation results are provided in Section III and we conclude in Section IV. Notations and symbols used in this paper are summarized in Table 1.

TABLE 1. Notation and symbols.

d	Dimension of the Hilbert space
$\boldsymbol{\rho}$	Density operator/matrix of a quantum state
$\boldsymbol{M}_n$	nth measurement operator
$\boldsymbol{I}$	Identity matrix
$\mathrm{tr}\,(\cdot)$	Trace operation
$(\cdot)^\dagger$	Conjugate transpose of an operator or of a vector
$\|u_{n,i}\rangle$	ith eigenvector of M_n
$a_{n,i}$	ith eigenvalue of M_n
$\mathcal{N}(\boldsymbol{\rho})$	Output state of the quantum depolarizing channel (QDC) when the input is $\boldsymbol{\rho}$
λ	Noise parameter for the QDC
$p_{n,i}$	Probability of obtaining measurement result corresponding to $\|u_{n,i}\rangle$ when measuring the noiseless state ρ
$p_{n,i}^{\mathrm{noisy}}$	Probability of obtaining measurement result corresponding to $\|u_{n,i}\rangle$ when measuring the noisy state $\mathcal{N}(\boldsymbol{\rho})$
$(\cdot)^T$	Transpose operation
$\boldsymbol{\Lambda}$	Transformation matrix of statistics of measurement results
$\boldsymbol{M}(\lambda)$	Expectation value of measurement operator $\boldsymbol{M}$ with noise λ
a_k	Richardson extrapolation constants
α_k	Noise amplification factor
N_{QST}	Number of copies of unknown quantum state to perform tomography measurement
N_{est}	Number of copies of basis states used to estimate λ
N_{ext}	Number of copies of unknown quantum state to obtain $\boldsymbol{M}(\alpha_1\lambda)$ in ZNE
N_{train}	Number of copies of random quantum states to generate training data set for neural network
N_{MEM}	Total number of measurements needed to perform QST with MEM, $N_{\mathrm{MEM}} = N_{\mathrm{QST}} + N_{\mathrm{est}}$
N_{ZNE}	Total number of measurements needed to perform QST with ZNE, $N_{\mathrm{ZNE}} = N_{\mathrm{QST}} + N_{\mathrm{ext}}$
N_{LS}	Total number of measurements needed to perform QST with LSEM, $N_{\mathrm{LS}} = N_{\mathrm{QST}} + N_{\mathrm{ext}} + N_{\mathrm{est}}$
N_{NN}	Total number of measurements needed to perform QST with neural network, $N_{\mathrm{NN}} = N_{\mathrm{QST}} + N_{\mathrm{train}}$
k	Number of different error parameters $\lambda_1, \lambda_2, \cdots, \lambda_k$ to perform LSEM-QST
L	Number of unique quantum states used to generate the training data set for neural network
$\mathcal{F}(\rho, \hat{\rho})$	Fidelity of the actual state and reconstructed state
$\mathrm{LSEM}_{1,2,3}$	Resource allocation scenario for LSEM-QST where ratio for N_{est} is $0.7, 0.5, 0.2$
r_{QST}	Ratio of N_{QST} to N_{MEM}
$N_{\{X,Y,Z\}}$	Number of copies of the unknown quantum states to obtain statistics of one measurement operator, $N_{\{X,Y,Z\}} = N_{\mathrm{QST}}/(d^2-1)$

II. QEM FOR QUANTUM STATE TOMOGRAPHY

The state of a quantum system is represented by a density operator, i.e., positive operator with a unit trace. Since the density operator itself is not an observable, we cannot readily obtain its matrix representation. Then, we have to measure several copies of the state of interest and construct the matrix representation from the statistics of the measurement outcomes. For reconstruction of a d-dimensional $\boldsymbol{\rho}$, at least $d^2 - 1$ measurement settings are required. Here, we used Gell-Mann bases measurement to simulate tomography measurements. Gell-Mann bases measurement is the generalization of Pauli measurements which consists of Pauli matrices $\{\boldsymbol{\sigma_x}, \boldsymbol{\sigma_y}, \boldsymbol{\sigma_z}\}$.

In the following, we briefly explain the LR QST. Let $\boldsymbol{M}_n$ be the measurement operator such as $\boldsymbol{M}_0 = \boldsymbol{I}$, $\mathrm{tr}(\boldsymbol{M}_n) = 0$ and $\mathrm{tr}(\boldsymbol{M}_m\boldsymbol{M}_n^\dagger) = 2\delta_{mn}$, where δ_{mn} is the Kronecker function. The $\boldsymbol{\rho}$ can be expressed as a linear combination of $\boldsymbol{M}_n$ as [34]

$$\boldsymbol{\rho} = \boldsymbol{I}/d + \sum_{n=1}^{d^2-1} r_n \boldsymbol{M}_n, \tag{1}$$

where $r_n = \mathrm{tr}(\boldsymbol{M}_n\boldsymbol{\rho})/2$. Suppose eigenvectors of $\boldsymbol{M}_n$ are denoted as $|u_{n,i}\rangle$ with its eigenvalues $a_{n,i}$, then $\boldsymbol{M}_n$ can be expressed in its spectral decomposition form as

$$\boldsymbol{M}_n = \sum_{i=1}^{d} a_{n,i} |u_{n,i}\rangle\langle u_{n,i}|, \tag{2}$$

where $\sum_i^d |u_{n,i}\rangle\langle u_{n,i}| = \boldsymbol{I}$. We can further write

$$|u_{n,i}\rangle\langle u_{n,i}| = \boldsymbol{I}/d + \sum_{k=1}^{d^2-1} \psi_{k,n}^i \boldsymbol{M}_k, \tag{3}$$

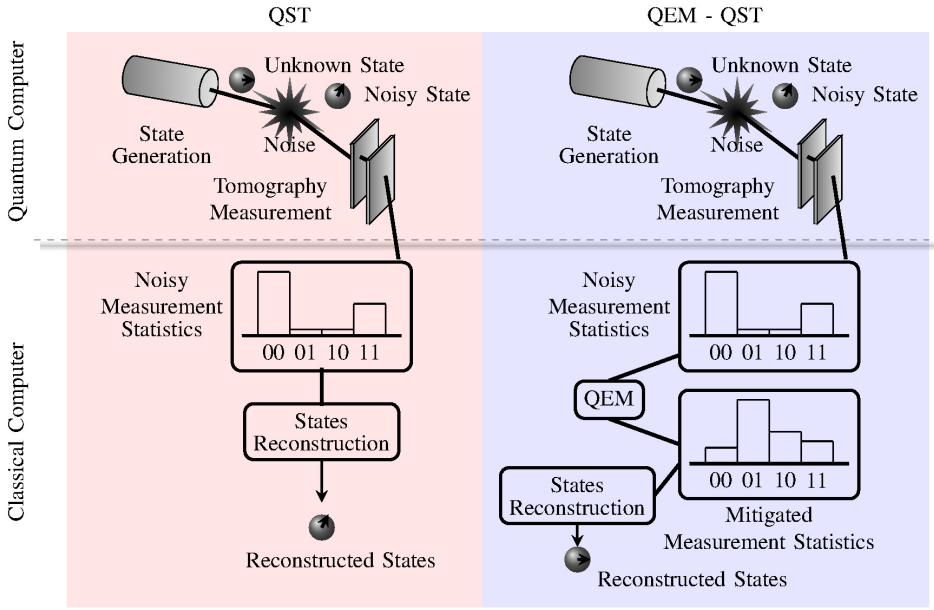

FIGURE 1. Illustration of QST without (left panel) and with (right panel) QEM implementation. When performing the QST without the QEM in a noisy environment, the reconstructed state will be close to the noisy state hence leads to low fidelity reconstructed state. In QST with QEM implementation, the noisy measurement statistics are mitigated to the noise-free statistics. The mitigated measurement statistics are then used to reconstruct the unknown quantum state.

where $\psi^i_{k,n} = \mathrm{tr}\left(|u_{n,i}\rangle\langle u_{n,i}|\boldsymbol{M}_k\right)/2$. The ideal probability of obtaining a measurement result $a_{n,i}$ when measuring $\boldsymbol{M}_n$ is

$$\begin{aligned} p_{n,i} &= \mathrm{tr}\left(|u_{n,i}\rangle\langle u_{n,i}|\rho\right) \\ &= \mathrm{tr}\left[\left(\boldsymbol{I}/d + \sum_{k=1}^{d^2-1}\psi^i_{k,n}\boldsymbol{M}_k\right)\boldsymbol{\rho}\right] \\ &= \frac{1}{d}\mathrm{tr}\left(\boldsymbol{\rho}\right) + \mathrm{tr}\left(\sum_{k=1}^{d^2-1}\psi^i_{k,n}\boldsymbol{M}_k\boldsymbol{\rho}\right) \\ &= \frac{1}{d} + \sum_{k=1}^{d^2-1}\phi^i_{k,n}r_k = \frac{1}{d} + \boldsymbol{\phi_{n,i}r} \end{aligned} \tag{4}$$

where $\phi^i_{k,n} = \mathrm{tr}\left(|u_{n,i}\rangle\langle u_{n,i}|\boldsymbol{M}_k\right)$ and r_k is the coefficient in (1). We can write (4) for all measurement results in the matrix form as

$$\boldsymbol{Y} = \boldsymbol{\Phi r}, \tag{5}$$

where the column vector $\boldsymbol{Y} = \left[p_{1,1} - \frac{1}{d}, \cdots, p_{n,d} - \frac{1}{d}\right]^T$ and matrix $\boldsymbol{\Phi} = \left[\boldsymbol{\phi_{1,1}}, \cdots, \boldsymbol{\phi_{n,d}}\right]^T$.

Once we measure each $\boldsymbol{M}_n$ and obtain estimates $\hat{p}_{n,i}$ of the probabilities $p_{n,i}$, we can obtain an estimate $\hat{\boldsymbol{Y}}$ of $\boldsymbol{Y}$. Then, $\boldsymbol{r}$ is estimated by,

$$\hat{\boldsymbol{r}} = \left(\boldsymbol{\Phi}^T\boldsymbol{\Phi}\right)^{-1}\boldsymbol{\Phi}^T\hat{\boldsymbol{Y}}.$$

Finally, the estimate $\hat{\boldsymbol{\rho}}$ of $\boldsymbol{\rho}$ can be obtained by substituting the elements of $\hat{\boldsymbol{r}}$ in (1).

The noisy evolution of quantum states is characterized by quantum channels. Mathematically, quantum channels are the completely positive trace-preserving maps on the set of density matrices. We consider a noisy setup where the noise is modeled by the quantum depolarizing channel (QDC) [35]. The QDC acts on a d-dimensional state $\boldsymbol{\rho}$ as

$$\mathcal{N}\left(\boldsymbol{\rho}\right) = \left(1-\lambda\right)\boldsymbol{\rho} + \lambda\boldsymbol{\pi}, \tag{6}$$

where $\boldsymbol{\pi} = \boldsymbol{I}/d$ is the d-dimensional maximally mixed state and $\lambda \in \left(0, 1 + \frac{1}{(d^2-1)}\right)$ is a real parameter. It is simple to see that the output of the QDC is the maximally mixed state when $\lambda = 1$. In this paper, we restrict the parameter λ to be in the interval $(0, 1)$ such that we obtain noiseless and the maximally mixed states at the boundaries of this interval and hence we can think of λ as the noise strength.

The probability of obtaining measurement result of $\mathcal{N}\left(\boldsymbol{\rho}\right)$ corresponding to $|u_{n,i}\rangle\langle u_{n,i}|$ is

$$\begin{aligned} p^{\mathrm{noisy}}_{n,i} &= \mathrm{tr}\left(\mathcal{N}\left(\boldsymbol{\rho}\right)|u_{n,i}\rangle\langle u_{n,i}|\right) \\ &= \mathrm{tr}\left(\left(\boldsymbol{\pi} + \left(1-\lambda\right)\boldsymbol{\rho}\right)|u_{n,i}\rangle\langle u_{n,i}|\right) \\ &= \frac{\lambda}{d} + \left(1-\lambda\right)p_{n,i} \neq p_{n,i}, \end{aligned} \tag{7}$$

where $p^{\mathrm{noisy}}_{n,i}$ denotes the elements of distribution of the noisy measurement results. Hence, if we perform QST with $p^{\mathrm{noisy}}_{n,i}$, the reconstructed states $\hat{\boldsymbol{\rho}}_{\mathrm{noisy}}$ will be less accurate than $\hat{\boldsymbol{\rho}}$. To obtain the reconstructed quantum states with high fidelity despite the noisy environment, we perform QEM to mitigate the effects of noise in the measurement results. The illustration of QEM implementation in QST can be seen in Fig. 1. Here we present some QEM methods to correct the noisy

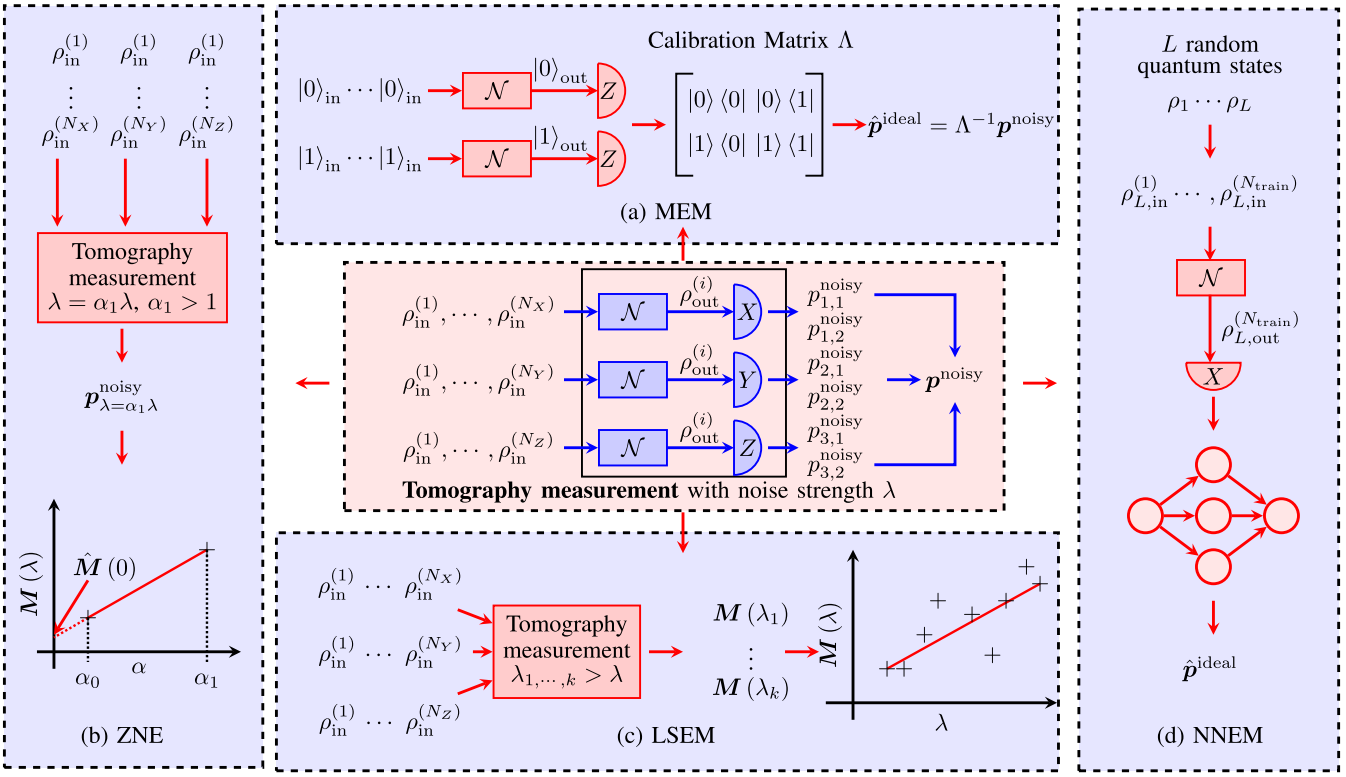

FIGURE 2. An overview of QST with different QEM schemes. A QST measurement setup with channel noise $\mathcal{N}$ is shown in the center panel. The measurement results $\hat{p}^{\text{noisy}}$ are fed to one of the QEM schemes to obtain the estimation of ideal measurement results $\hat{p}^{\text{ideal}}$. The $\hat{p}^{\text{ideal}}$ are then used to reconstruct the unknown noiseless quantum state. Subfigures (a) MEM, (b) ZNE, (c) LSEM, and (d) NNEM demonstrate the main ideas of the QEM schemes that we consider here. See Section II-A, Section II-B, Section II-C, and Section II-D, respectively, for details of each of these methods.

measurement probability results before reconstructing the states.

Both QST and QEM need many quantum resources to perform well. Since each of the QEM methods requires different kind of resources in mitigating the errors, in this work we define the resources as the number of quantum states utilized either they are the unknown $\boldsymbol{\rho}$ or states other than $\boldsymbol{\rho}$ e.g. $|0\rangle$.

A. MEASUREMENT ERROR MITIGATION

The measurement error mitigation (MEM) [27] is used to mitigate the errors introduced by a noisy measurement device. However, as we demonstrate in the following, the formalism of MEM can also be used to mitigate the effects of some noisy channels, e.g., the QDC considered here. A pictorial depiction of MEM is shown in Fig. 2(a).

Let $\boldsymbol{p}^{\text{ideal}}$ and $\boldsymbol{p}^{\text{noisy}}$ denote the probability vectors of measurement statistics from an ideal and noisy measurement device, respectively. The relation between $\boldsymbol{p}^{\text{ideal}}$ and $\boldsymbol{p}^{\text{noisy}}$ is shown as

$$\boldsymbol{p}^{\text{noisy}} = \boldsymbol{\Lambda}\boldsymbol{p}^{\text{ideal}}, \tag{8}$$

where $\boldsymbol{\Lambda}$ is a left stochastic transformation matrix.

Let us consider the example of a noisy measurement device that gives the correct measurement outcome with probability $1 - \lambda + \lambda/d$ and randomly clicks one of the remaining detectors with probability λ/d each. This specific noisy measurement is characterized by

$$\boldsymbol{\Lambda} = \begin{bmatrix} 1-\lambda+\lambda/d & \lambda/d & \cdots & \lambda/d \\ \lambda/d & 1-\lambda+\lambda/d & \cdots & \lambda/d \\ \vdots & \vdots & \ddots & \vdots \\ \lambda/d & \lambda/d & \cdots & 1-\lambda+\lambda/d \end{bmatrix}. \tag{9}$$

On the other hand, by inspecting (7), it is clear that (9) also provides the relation between $p_{n,i}$ and $p_{n,i}^{\text{noisy}}$. Therefore, we can use the framework of measurement errors to characterize and *mitigate* the errors introduced by a QDC followed by a noiseless measurement device.

Note that quantum noise (6) is generally an irreversible process. However, (9) represents the transformation of the measurement statistics which is a reversible process. Thus, the mitigated measurement results can be expressed as

$$\hat{\boldsymbol{p}}^{\text{ideal}} = \boldsymbol{\Lambda}^{-1}\boldsymbol{p}^{\text{noisy}}. \tag{10}$$

In this work, we mitigate the measurement results directly from (7) as

$$\hat{p}_{n,i} = \frac{1}{1-\hat{\lambda}}\left(p_{n,i}^{\text{noisy}} - \frac{\hat{\lambda}}{d}\right). \tag{11}$$

To this end, we first estimate the strength λ of QDC. The estimate $\hat{\lambda}$ is obtained by passing $N_{|0\rangle}$ copies of $|0\rangle$ to the

channel described in (6) and performing Z basis measurement on the output of the channel [36]. Then, λ can be estimated by

$$\hat{\lambda} = dp_1, \tag{12}$$

where p_1 is the probability of measurement result corresponding to $|1\rangle\langle 1|$.

Let N_{est} and N_{QST} denote the number of measurements utilized for estimating λ and for the QST, respectively. Then, the total number of measurements performed for the QST with the MEM N_{MEM} is $N_{\text{est}} + N_{\text{QST}}$. During the QST step, all N_{QST} copies are equally divided among all measurement operators $\boldsymbol{M}_n$.

B. ZERO-NOISE EXTRAPOLATION

Zero-noise extrapolation (ZNE) is based on Richardson's extrapolation method to extrapolate the noise-free expectation value of an observable $\boldsymbol{M}$ [20]. We can represent the expectation of $\boldsymbol{M}$ as a series in λ as [20]

$$\boldsymbol{M}(\lambda) = \boldsymbol{M}(0) + \sum_{k}^{n} a_k \lambda^k + O\left(\lambda^{n+1}\right), \tag{13}$$

where λ, $\boldsymbol{M}(\lambda)$ and a_k denote noise strength, expectation value of $\boldsymbol{M}$ with noise λ and the model-specific constants, respectively.

ZNE order-n in noisy QST with noise parameter λ is performed by measuring many copies of the unknown quantum state with amplified noise strength $\alpha_k\lambda$ where $\{\alpha_0 < \alpha_1 < \cdots < \alpha_n | \alpha_0 = 1\}$. It has been proved that if the noise is invariant, one can get the measurement at amplified noise by stretching the gate times and perform the measurement on the output [20]. Another possible strategy is by inserting some additional noisy gates (identity insertion) in the quantum circuit [23], [37] and then measuring the output.

The estimation of noise-free expectation value $\boldsymbol{M}(0)$ if the noise is amplified by the work in [20] can be calculated as

$$\boldsymbol{M}(0) = \frac{\alpha_1}{\alpha_1 - \alpha_0}\boldsymbol{M}(\lambda) + \frac{\alpha_0}{\alpha_0 - \alpha_1}\boldsymbol{M}(\alpha_1\lambda), \tag{14}$$

where we have used the linear extrapolation with one additional noise strength $\alpha_1\lambda$. Thus, the mitigated measurement result $\boldsymbol{M}(0)$ is dependent on noisy measurement results and amplification factors only. The illustration of ZNE order-1 is portrayed in Fig. 2(b).

The error mitigation by ZNE is proposed and discussed in the context of expectation value of an observable $\boldsymbol{M}$ with respect to some state $\boldsymbol{\rho}$, i.e., $\mathbb{E}\{\boldsymbol{M}\}_\rho = \text{tr}(\boldsymbol{M}\rho)$. The measurement outcome probabilities $p_{n,i}$ have exactly the same mathematical structure, i.e., $p_{n,i} = \text{tr}\left(\rho\Pi_{n,i}\right)$, where $\Pi_{n,i} = |u_{n,i}\rangle\langle u_{n,i}|$. Therefore, we can use the ZNE error mitigation technique as effectively for mitigating the errors in measurement probabilities in the QST problem.

The total measurements needed to perform QST with ZNE order-1 is N_{ZNE} which includes N_{QST} and N_{ext} copies of the unknown quantum states to obtain the noisy measurement results at noise λ and the amplified noise $\alpha_1\lambda$, respectively.

C. LEAST SQUARE ERROR MITIGATION

The least square error mitigation (LSEM) was proposed in [29]. The main idea of LSEM (shown in Fig. 2(c)) is to estimate the expectation of $\boldsymbol{M}$ at multiple random noise levels, followed by the least square fitting of these data points. The extension (extrapolation) of this least square fitted curve to the zero-noise value estimates the noise-free expectation of $\boldsymbol{M}$. The main difference between the ZNE and the LSEM is as follows. The ZNE is performed by extrapolating an nth order polynomial over $(n+1)$ data points. On the other hand, the degree of the fitting polynomial and the number of data points in LSEM are independent of each other. The only consideration is that the number of data points must be greater than the degree of polynomial we target for fitting. By considering multiple data points for the least square fitting reduces the finite sample effects and other uncertainties in the expectation values of $\boldsymbol{M}$ in the fitted curve.

To perform error mitigation for QST with noise parameter λ_1 by the least square fitting, we subject the unknown quantum state under study to various noise strengths $(\lambda_2, \lambda_3, \cdots, \lambda_k)$ where $\lambda_i > \lambda_1$ and perform measurements for each λ_i. The Richardson extrapolation order-n for k number of noise parameters can be written as linear equation,

$$\begin{aligned} \boldsymbol{P}^* &= \boldsymbol{\lambda}\boldsymbol{A} \\ \begin{bmatrix} \boldsymbol{M}(\lambda_1) \\ \boldsymbol{M}(\lambda_2) \\ \vdots \\ \boldsymbol{M}(\lambda_k) \end{bmatrix} &= \begin{bmatrix} 1 & \lambda_1^1 & \cdots & \lambda_1^n \\ 1 & \lambda_2^1 & \cdots & \lambda_2^n \\ \vdots & \vdots & \ddots & \vdots \\ 1 & \lambda_k^1 & \cdots & \lambda_k^n \end{bmatrix} \begin{bmatrix} \boldsymbol{M}(0) \\ a_1 \\ \vdots \\ a_n, \end{bmatrix} \end{aligned} \tag{15}$$

where $\boldsymbol{M}(\lambda_i)$ denotes the expectation of $\boldsymbol{M}$ with noise strength λ_i. The system (15) is an overdetermined set of equations whose least square solution for $\boldsymbol{A}$ is

$$\boldsymbol{A} = \boldsymbol{\lambda}^+ \boldsymbol{P}^*, \tag{16}$$

where $\boldsymbol{\lambda}^+ = \left(\boldsymbol{\lambda}^T\boldsymbol{\lambda}\right)^{-1}\boldsymbol{\lambda}^T$ is the Moore-Penrose pseudo-inverse of $\boldsymbol{\lambda}$. The mitigated measurement result will be the first element of vector $\boldsymbol{A}$.

The QST with LSEM needs to perform N_{LS} measurements to measure quantum resources consists of N_{QST} and N_{ext} copies of quantum states under study to generate vector $\boldsymbol{P}^*$ and N_{est} copies of $|0\rangle$ to estimate k number of λ.

D. NEURAL NETWORK BASED ERROR MITIGATION

Previous work on reducing state-preparation-and-measurements (SPAM) errors in QST by implementing a deep neural network (DNN) was proposed in [15]. The neural network was trained to discover the patterns of the true measurement probabilities and the experimental results. Suppose $\boldsymbol{p}^{\text{noisy}}$ and $\boldsymbol{p}^{\text{ideal}}$ denotes the noisy and the ideal true probability vectors corresponding to $\boldsymbol{M}$. We want to learn the relationship between $\boldsymbol{p}^{\text{noisy}}$ and $\boldsymbol{p}^{\text{ideal}}$ through neural network. For $d = 6$, the neural network has 36 input parameters which are the noisy measurement probability results, and 36 output parameters which are the ideal measurements probability

from symmetric informationally complete [38] measurement, 400 nodes for the first hidden layer and 200 nodes for the second hidden layer. The network is trained with RMSprop optimizer and the loss function to be minimized during the training process is the Kullback-Leibler divergence (KLD). The hidden layer and output layer nodes possess rectified linear unit and softmax function, respectively. After the network is well trained, we can use the model to get the estimation of ideal measurement probabilities from new noisy measurement data.

In this work, we use Gell-Mann bases measurement as we stated in the previous section. Rather than feeding the network with measurement results from all measurement operators, we train the network for each measurement operator. For example, for the $\boldsymbol{M}_n$ and $d = 2$, the $p_{n,1}^{\text{noisy}}$ or $p_{n,2}^{\text{noisy}}$ is used as the training input of the network. Therefore the input layer and output layer will have one node each. The hidden layer and output layer nodes possess rectified linear unit and linear activation function, respectively. We train the network with stochastic gradient descent (SGD) optimizer and the loss function to be minimized during the training process is the mean absolute error. If the channel is depolarizing channel, we can train the network for one measurement operator only and use the model obtained to estimate the probability of other measurement operators.

For NN based error mitigation, we need to perform N_{NN} measurements to measure N_{train} number of resources for the NN training process and N_{QST} copies of unknown quantum states to collect information regarding the states.

Before moving to the numerical examples, we remark that it is possible to transform any other noise model, e.g., amplitude damping or phase damping, into a depolarizing channel by twirling [28]. Furthermore, all the considered QEM schemes have been demonstrated for different noise models. For example, the MEM has been shown to work for Pauli and generalized Pauli channels in [39]. In [20], the ZNE has been demonstrated on the depolarizing, amplitude damping, and phase damping channels. The LSEM has been demonstrated for the amplitude damping and the phase damping channels in [29]. In summary, it is possible to utilize these QEM schemes for the task of QST even if the noise is not of the depolarizing form. If twirling is utilized for their application, the performance of the QST will be exactly the same as discussed here since the effective channel will of depolarizing form. However, the exact analysis without twirling can be a topic of some future studies.

III. NUMERICAL EXAMPLES

In this section, we provide numerical examples of the aforementioned QEM schemes for QST. We assume that the state $\boldsymbol{\rho}$ generated from the unknown source is subject to QDC $\mathcal{N}$ of strength λ. Then, we perform the measurement of $\mathcal{N}(\rho)$ and attempt to recover the original state $\boldsymbol{\rho}$ from the noisy measurement results. The scheme of our work can be seen in Fig. 1 and the scheme for each QEM method is illustrated in Fig. 2. Since different QEM methods require different resources, it is difficult to directly compare them in terms of resources. For example if N copies of $\boldsymbol{\rho}$ are available, MEM can utilize all of these copies for the QST while requiring N_{est} copies of some known state, e.g., $|0\rangle$ to characterize the transformation matrix $\boldsymbol{\Lambda}$. This is in contrast with the ZNE method where we have to split the N copies of $\boldsymbol{\rho}$ into N_{QST} and N_{ext} for the error mitigation to be possible. This makes it challenging to properly compare the different QEM methods. For the sake of comparison, we count the total number of times we have to measure *any* state in the setup as the resource. That is, we count the total number of quantum states—known, e.g., $|0\rangle$ or unknown $\boldsymbol{\rho}$—as our resource. Then, we fix the total number of resources for each QEM method and compare their performance.

We use the infidelity between actual state $\boldsymbol{\rho}$ and reconstructed state $\hat{\boldsymbol{\rho}}$ to quantify the performance of QST with error mitigation. Infidelity is defined as

$$1 - \mathcal{F}\left(\boldsymbol{\rho}, \hat{\boldsymbol{\rho}}\right) = 1 - \text{tr}\left(\sqrt{\sqrt{\boldsymbol{\rho}}\hat{\boldsymbol{\rho}}\sqrt{\boldsymbol{\rho}}}\right) \tag{17}$$

where $\mathcal{F}\left(\boldsymbol{\rho}, \hat{\boldsymbol{\rho}}\right)$ denotes the fidelity between $\boldsymbol{\rho}$ and $\hat{\boldsymbol{\rho}}$. We perform numerical simulations to compare the performance of various error mitigation methods in QST by using the 10^5 resources for each QEM method. We plot the performance plots by averaging the infidelity at each point over 10^4 random Bures mixed state.

Fig. 3 shows the average infidelity of the mixed states mitigated with MEM as a function of λ and $r_{\text{QST}} = N_{\text{QST}}/\left(N_{\text{QST}} + N_{\text{est}}\right)$ for $d = 2$. For example, if the ratio of N_{QST} and N_{est} is $0.3 : 0.7$, $30,000$ copies of ρ are used to collecting the information of the states and $70,000$ copies of $|0\rangle$ are used to estimate the λ. Since we used the Gell-Mann bases measurement, the expectation value of each measurement operator $\left(\sigma_x, \sigma_y, \sigma_z\right)$ is obtained by performing $10,000$ $\left(N_{\text{QST}}/3\right)$ measurements for each operator. From the Fig. 3, we observe that the $N_{\text{QST}} : N_{\text{est}} = 0.8 : 0.2$ and $N_{\text{QST}} : N_{\text{est}} = 0.7 : 0.3$ have the similar performance in

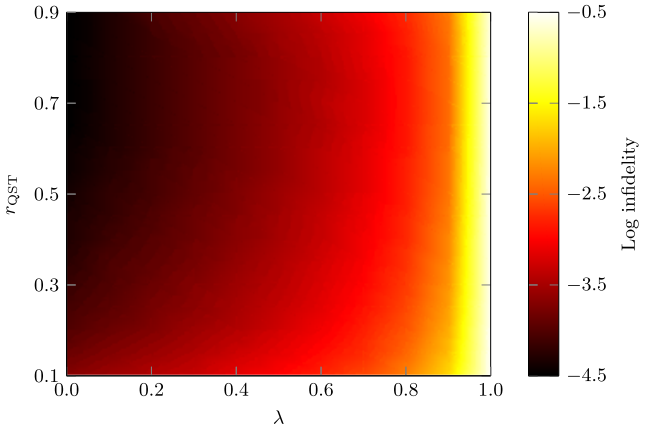

FIGURE 3. Performance of MEM. Average infidelity of reconstructed and actual quantum states as a function of $r_{\text{QST}} = N_{\text{QST}}/\left(N_{\text{QST}} + N_{\text{est}}\right)$ and λ by using $N_{\text{MEM}} = 10^5$ resources for $d = 2$.

mitigating the error in noisy measurement result. However, the $N_{\text{QST}} : N_{\text{est}} = 0.8 : 0.2$ gives a more better result for really small noise than the $N_{\text{QST}} : N_{\text{est}} = 0.7 : 0.3$ since it uses more resources to perform the QST. On the other side, when N_{est} is allocated a substantial amount of resources, it cannot perform better than the other allocation schemes. If we allocate most of the available resources to infer λ, then we will get a reconstructed state with low fidelity.

Fig. 4(a) shows the average infidelity of QST with ZNE order-1 as a function of λ for mixed states with $d = 2$ and $\alpha_1 = 5$ for $0 \leq \lambda \leq 0.2$ and $\frac{1}{\lambda}$ for $0.2 < \lambda \leq 1$. We observe that allocating 70% of the resources to QST and the rest to obtain data points for the extrapolation is the best resources allocation scheme to reconstruct the noise-free quantum states with ZNE. To demonstrate the effect of α_1 in QST performances, we plot the infidelity for different α_1 in Fig. 4(b) with $N_{\text{QST}} = N_{\text{ext}} = 5 \times 10^4$. From the simulation result, we can see that if we make the circuit noisier, the QST with ZNE is giving a similar result with MEM in Fig. 3.

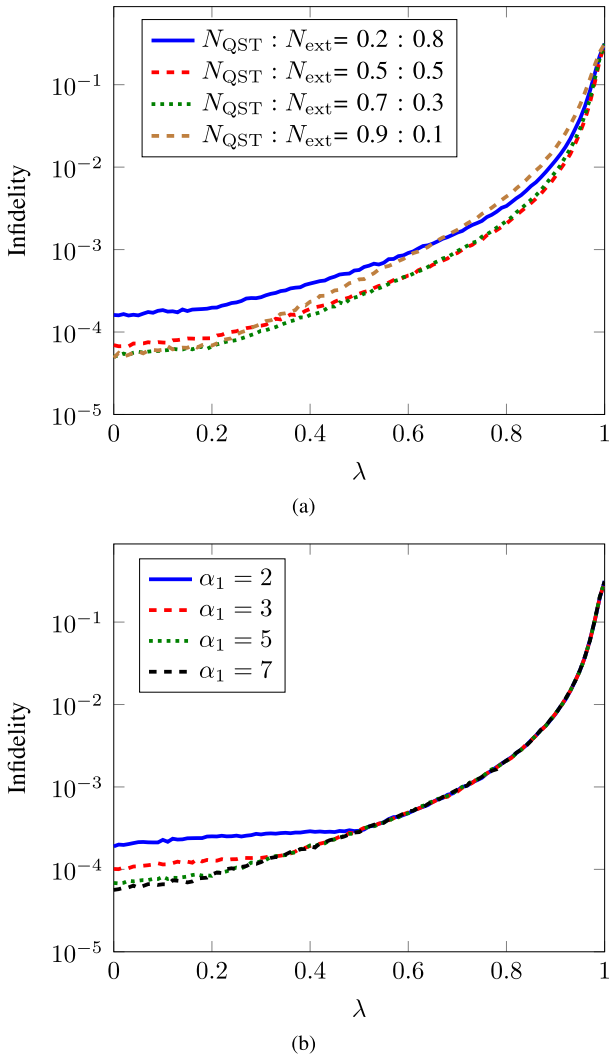

FIGURE 4. Performance of ZNE. Average infidelity of reconstructed and actual quantum states by using $N_{\text{ZNE}} = 10^5$ resources for $d = 2$ as a function of λ for (a) $\alpha_1 = 5$ and various N_{QST} and N_{ext} ratio and (b) various α_1 with $N_{\text{QST}} : N_{\text{ext}} = 0.5 : 0.5$.

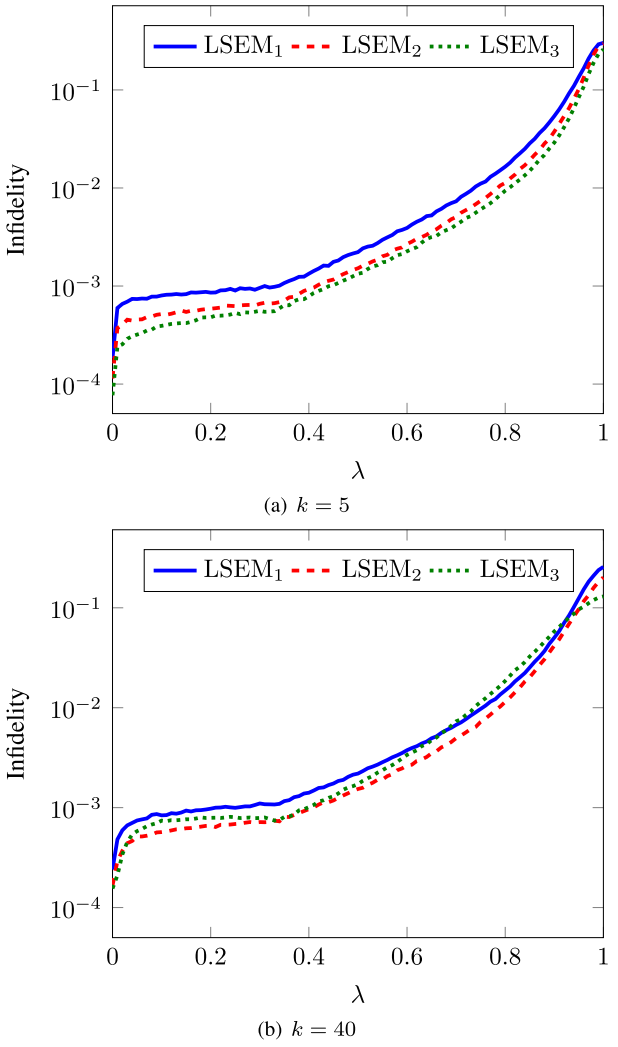

FIGURE 5. Performance of LSEM. Average infidelity of reconstructed and actual quantum states as a function of λ with LSEM for $k = 5, 40$ random λ_i and various resources allocation ratios.

Fig. 5 shows the infidelity of QST with LSEM for different number of random noise parameters k and different resource allocation scheme $\text{LSEM}_1, \text{LSEM}_2, \text{LSEM}_3$. The $\text{LSEM}_{\{1,2,3\}}$ refers to resources allocation scheme where the ratio of $N_{\text{est}} = 0.7, 0.5, 0.2$ respectively. The rest of the resources are divided equally among all measurement operators and k to construct the vector $\boldsymbol{P}^*$. For example, if we use scheme 1 and $k = 5$, 70% of the resources are used to estimate five λ_i and the rest are used to measure the $\boldsymbol{\rho}$ for five λ_i. Thus, to mitigate the noisy measurement result of one measurement operator $2,000$ $(30,000/(3 \times 5))$ copies of the unknown states are needed to obtain the elements of $\boldsymbol{P}^*$ and $14,000$ copies of $|0\rangle$ are used to estimate λ_i. It can be observed that scheme 3 with $k = 5$ gives the best performance among all schemes.

Fig. 6 shows the average infidelity of QST with neural network based QEM for $d = 2$ where the hidden layer of the neural network has 20 nodes. We divided the available 10^5 resources into $N_{\text{QST}} : N_{\text{train}} = 0.1 : 0.9$ thus $3,333$ $(10,000/3)$ copies are used to obtain the measurement results of $\boldsymbol{\rho}$ under study and $L = 27$ random quantum states are used for generating the training data set where $3,333$ copies of each random states are used to obtain the statistics of each $\boldsymbol{M}_n$. The more the copies are used to obtain information about the $\boldsymbol{\rho}$, the less the sample L can be used in the neural network training process.

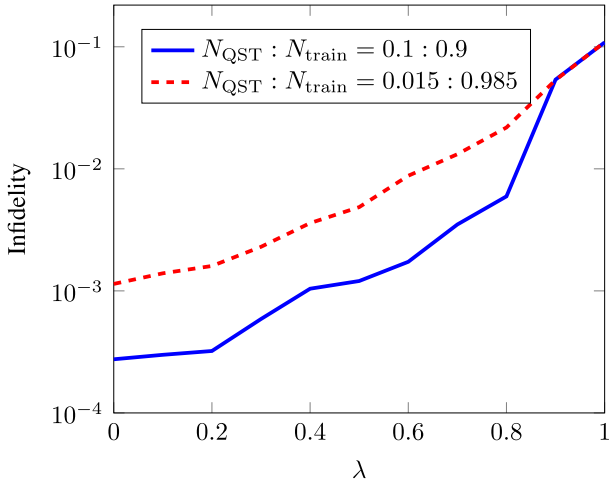

FIGURE 6. Performance of NNEM. Average infidelity of reconstructed quantum states as a function of λ mitigated with NN for $d = 2$.

To compare the performance of all QEM methods we have simulated, we plot the best result of each QEM method in Fig. 7. The MEM plotted is the one with $N_{\text{QST}} : N_{\text{est}} = 0.8 : 0.2$ where $N_{\text{QST}} = 80,000$ and $N_{\text{est}} = 20,000$ copies. The best result observed for ZNE is $N_{\text{QST}} : N_{\text{ext}} = 0.7 : 0.3$ with $\alpha_1 = 7$. For QST and extrapolation part, the copies of $\boldsymbol{\rho}$ used are $70,000$ and $30,000$ copies, respectively. For LSEM, we plotted the scheme 3 where $k = 5$. For neural network based error mitigation, the resource allocation ratio used is $N_{\text{QST}} : N_{\text{train}} = 0.1 : 0.9$. The parameter values for Fig. 7 are given in Table 2 where $N_\rho, N_{|0\rangle}, N_{\text{rand}}$ denote the copies of ρ, copies of $|0\rangle$ and copies of random quantum states, respectively. From the picture, we can see that MEM and ZNE give similar performance in mitigating the error in noisy measurement results, while LSEM and NN have similar results but the NN has a higher variance than LSEM.

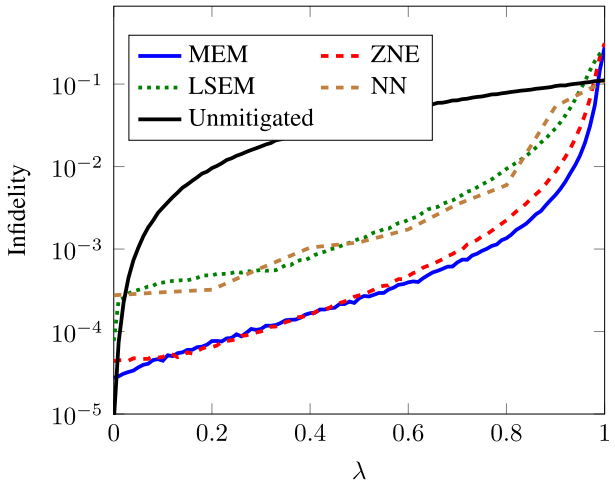

FIGURE 7. Comparison of different QEM schemes with optimal resource allocation. Average infidelity of reconstructed states as a function of the depolarizing noise strength λ for the best implementations of different QEM methods.

To see the performance of each error mitigation method if we use the same number of N_{QST}, we perform simulation where $\lambda = 0.4$ and $N_{\{X,Y,Z\}} = N_c = 10^2, 10^3, 10^4, 10^5$ and plot the result in Fig. 8(a). The ratio of resources for QST measurement and QEM is based on the simulation result

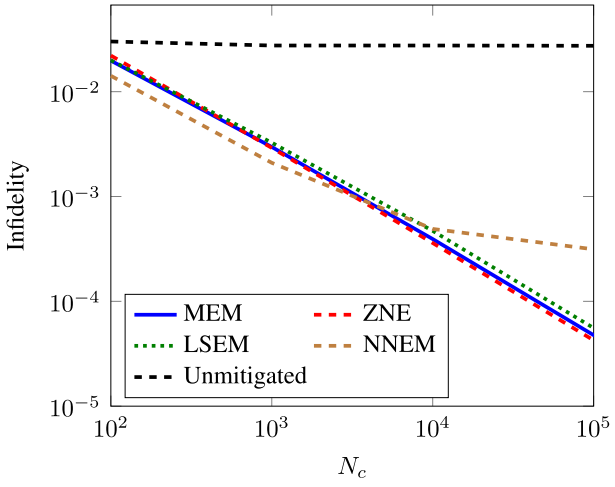

(a) $N_{\text{MEM}} \neq N_{\text{ZNE}} \neq N_{\text{LS}} \neq N_{\text{NN}}$

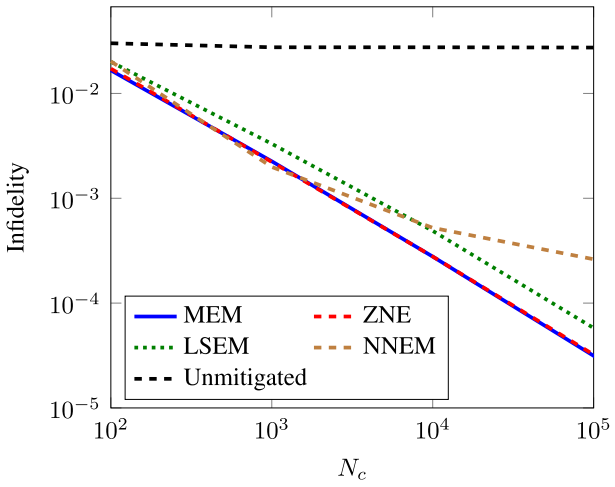

(b) $N_{\text{MEM}} = N_{\text{ZNE}} = N_{\text{LS}} = N_{\text{NN}}$

FIGURE 8. Comparison of different QEM schemes with the fixed number of total resources. (a) Average infidelity of reconstructed mitigated quantum states for different QEM methods by using the same number of N_{QST} but different individually optimal resources for each scheme and (b) with the same number of N_{QST} and total resources where $\lambda = 0.4$.

TABLE 2. Details of resource allocation for QST and QEM.

			MEM	ZNE	LSEM	NNEM	Unmitigated
Fig. 7	QST	N_ρ	8.0×10^4	7.0×10^4	1.6×10^4	1.0×10^4	1.0×10^5
	QEM	$N_{\|0\rangle}$	2.0×10^4		2.0×10^4		
		N_ρ		3.0×10^4	6.4×10^4		
		N_{rand}				9.0×10^4	
Total			$\mathbf{1.0 \times 10^5}$	$\mathbf{1.0 \times 10^5}$	$\mathbf{1.0 \times 10^5}$	$\mathbf{1.0 \times 10^5}$	$\mathbf{1.0 \times 10^5}$
Fig. 8(a)	QST	N_ρ	3.0×10^3	3.0×10^3	3.0×10^3	3.0×10^3	3.0×10^3
	QEM	$N_{\|0\rangle}$	7.5×10^2		3.7×10^3		
		N_ρ		1.3×10^3	1.2×10^4		
		N_{rand}				2.7×10^4	
Total			$\mathbf{3.7 \times 10^3}$	$\mathbf{4.3 \times 10^3}$	$\mathbf{1.9 \times 10^4}$	$\mathbf{3.0 \times 10^4}$	$\mathbf{3.0 \times 10^3}$
Fig. 8(b)	QST	N_ρ	3.0×10^3	3.0×10^3	3.0×10^3	3.0×10^3	3.0×10^3
	QEM	$N_{\|0\rangle}$	6.0×10^3		3.6×10^3		
		N_ρ		6.0×10^3	2.4×10^3		
		N_{rand}				6.0×10^3	
Total			$\mathbf{9.0 \times 10^3}$	$\mathbf{9.0 \times 10^3}$	$\mathbf{9.0 \times 10^3}$	$\mathbf{9.0 \times 10^3}$	$\mathbf{3.0 \times 10^3}$

in Fig. 7, thus the number of total resources of QEM methods are different ($N_{\text{MEM}} \neq N_{\text{ZNE}} \neq N_{\text{LS}} \neq N_{\text{NN}}$). From the figure, we can see that if we do not perform QEM in QST, even though we increase the N_{QST}, we cannot increase the fidelity of the reconstructed states as shown by the dashed black line. The NN outperforms the other QEM methods when $N_c < 10^4$ but shows no big improvement when we increase the N_c. Despite using more resources than MEM and ZNE, LSEM cannot give better fidelity than both methods. Fig. 8(b) shows the infidelity of reconstructed and actual states where N_{QST} and total resources are the same for each QEM method. The total resources used are $9 \times 10^2, 9 \times 10^3, 9 \times 10^4, 9 \times 10^5$. We report the parameter values used in Fig. 8 (for $N_{\text{QST}} = 3 \times 10^3$) in Table 2. We can see that by using the same total resources and QST measurement number, MEM and ZNE gives the best result among other QEM methods under study.

IV. CONCLUSION

We have demonstrated the efficacy of QEM schemes for the task of QST in the presence of noise. We provided the implementation of different QEM methods for noisy QST where the noise is modeled as the depolarizing channel. With the help of QEM, we were able to reduce the errors caused by the noisy environment, thus improving the fidelity between the obtained density matrix and the true quantum state. Our considered scenario reveals the MEM and the ZNE to be the most effective QEM methods, recovering almost the original fidelities for small noise values. Future works may include the QEM for process tomography and other quantum information processing tasks.

REFERENCES

[1] G. Mauro D'Ariano, M. G. Paris, and M. F. Sacchi, "Quantum tomography," *Adv. Imag. Electron Phys.*, vol. 128, pp. 206–309, Feb. 2003.

[2] Y.-X. Liu, L. F. Wei, and F. Nori, "Tomographic measurements on superconducting qubit states," *Phys. Rev. B, Condens. Matter*, vol. 72, no. 1, Jul. 2005, Art. no. 014547.

[3] K. Vogel and H. Risken, "Determination of quasiprobability distributions in terms of probability distributions for the rotated quadrature phase," *Phys. Rev. A, Gen. Phys.*, vol. 40, no. 5, p. 2847, Sep. 1989.

[4] D. M. Appleby, H. Yadsan-Appleby, and G. Zauner, "Galois automorphisms of a symmetric measurement," 2012, *arXiv:1209.1813*. [Online]. Available: http://arxiv.org/abs/1209.1813

[5] J. A. Smolin, J. M. Gambetta, and G. Smith, "Efficient method for computing the maximum-likelihood quantum state from measurements with additive Gaussian noise," *Phys. Rev. Lett.*, vol. 108, no. 7, 2012, Art. no. 070502.

[6] J. Shang, Z. Zhang, and H. K. Ng, "Superfast maximum-likelihood reconstruction for quantum tomography," *Phys. Rev. A, Gen. Phys.*, vol. 95, no. 6, Jun. 2017, Art. no. 062336.

[7] F. Huszár and N. M. T. Houlsby, "Adaptive Bayesian quantum tomography," *Phys. Rev. A, Gen. Phys.*, vol. 85, no. 5, May 2012, Art. no. 052120.

[8] C. Granade, J. Combes, and D. G. Cory, "Practical Bayesian tomography," *New J. Phys.*, vol. 18, no. 3, Mar. 2016, Art. no. 033024.

[9] D. S. Gonçalves, C. L. N. Azevedo, C. Lavor, and M. A. Gomes-Ruggiero, "Bayesian inference for quantum state tomography," *J. Appl. Statist.*, vol. 45, no. 10, pp. 1846–1871, Nov. 2017.

[10] B. Qi, Z. B. Hou, L. Li, D. Dong, G. Y. Xiang, and G. C. Guo, "Quantum state tomography via linear regression estimation," *Sci. Rep.*, vol. 3, Apr. 2013, Art. no. 3496.

[11] B. Qi, Z. Hou, Y. Wang, D. Dong, H.-S. Zhong, L. Li, G.-Y. Xiang, H. M. Wiseman, C.-F. Li, and G.-C. Guo, "Adaptive quantum state tomography via linear regression estimation: Theory and two-qubit experiment," *NPJ Quantum Inf.*, vol. 3, no. 1, pp. 1–7, Apr. 2017.

[12] G. Torlai, G. Mazzola, J. Carrasquilla, M. Troyer, R. Melko, and G. Carleo, "Neural-network quantum state tomography," *Nature Phys.*, vol. 14, no. 5, pp. 447–450, Feb. 2018.

[13] T. Xin, S. Lu, N. Cao, G. Anikeeva, D. Lu, J. Li, G. Long, and B. Zeng, "Local-measurement-based quantum state tomography via neural networks," *NPJ Quantum Inf.*, vol. 5, no. 1, pp. 1–8, Nov. 2019.

[14] S. Lohani, B. T. Kirby, M. Brodsky, O. Danaci, and R. T. Glasser, "Machine learning assisted quantum state estimation," *Mach. Learn., Sci. Technol.*, vol. 1, no. 3, Jul. 2020, Art. no. 035007.

[15] A. M. Palmieri, E. Kovlakov, F. Bianchi, D. Yudin, S. Straupe, J. D. Biamonte, and S. Kulik, "Experimental neural network enhanced quantum tomography," *NPJ Quantum Inf.*, vol. 6, no. 1, pp. 1–5, Feb. 2020.

[16] D. Bondarenko and P. Feldmann, "Quantum autoencoders to denoise quantum data," *Phys. Rev. Lett.*, vol. 124, no. 13, Mar. 2020, Art. no. 130502.

[17] T. Achache, L. Horesh, and J. Smolin, "Denoising quantum states with quantum autoencoders—Theory and applications," 2020, *arXiv:2012.14714*. [Online]. Available: http://arxiv.org/abs/2012.14714

[18] S. T. Merkel, J. M. Gambetta, J. A. Smolin, S. Poletto, A. D. Córcoles, B. R. Johnson, C. A. Ryan, and M. Steffen, "Self-consistent quantum process tomography," *Phys. Rev. A, Gen. Phys.*, vol. 87, no. 6, Jun. 2013, Art. no. 062119.

[19] S. Ahmed, C. S. Muñoz, F. Nori, and A. F. Kockum, "Classification and reconstruction of optical quantum states with deep neural networks," 2020, *arXiv:2012.02185*. [Online]. Available: http://arxiv.org/abs/2012.02185

[20] K. Temme, S. Bravyi, and J. M. Gambetta, "Error mitigation for short-depth quantum circuits," *Phys. Rev. Lett.*, vol. 119, no. 18, Nov. 2017, Art. no. 012338.
[21] S. Endo, S. C. Benjamin, and Y. Li, "Practical quantum error mitigation for near-future applications," *Phys. Rev. X*, vol. 8, no. 3, Jul. 2018, Art. no. 031027.
[22] Y. Li and S. C. Benjamin, "Efficient variational quantum simulator incorporating active error minimization," *Phys. Rev. X*, vol. 7, no. 2, Jun. 2017, Art. no. 021050.
[23] A. He, B. Nachman, W. A. de Jong, and C. W. Bauer, "Resource efficient zero noise extrapolation with identity insertions," 2020, *arXiv:2003.04941*. [Online]. Available: http://arxiv.org/abs/2003.04941
[24] A. Kandala, K. Temme, A. D. Córcoles, A. Mezzacapo, J. M. Chow, and J. M. Gambetta, "Error mitigation extends the computational reach of a noisy quantum processor," *Nature*, vol. 567, no. 7749, pp. 491–495, Mar. 2019.
[25] C. Hempel, C. Maier, J. Romero, J. McClean, T. Monz, H. Shen, P. Jurcevic, B. P. Lanyon, P. Love, R. Babbush, A. Aspuru-Guzik, R. Blatt, and C. F. Roos, "Quantum chemistry calculations on a trapped-ion quantum simulator," *Phys. Rev. X*, vol. 8, no. 3, Jul. 2018, Art. no. 031022.
[26] A. J. McCaskey, Z. P. Parks, J. Jakowski, S. V. Moore, T. D. Morris, T. S. Humble, and R. C. Pooser, "Quantum chemistry as a benchmark for near-term quantum computers," *NPJ Quantum Inf.*, vol. 5, no. 1, pp. 1–8, Nov. 2019.
[27] F. B. Maciejewski, Z. Zimborás, and M. Oszmaniec, "Mitigation of readout noise in near-term quantum devices by classical post-processing based on detector tomography," *Quantum*, vol. 4, p. 257, Apr. 2020.
[28] H. Kwon and J. Bae, "A hybrid quantum-classical approach to mitigating measurement errors in quantum algorithms," *IEEE Trans. Comput.*, early access, Jul. 16, 2020, doi: 10.1109/TC.2020.3009664.
[29] M. Otten and S. K. Gray, "Recovering noise-free quantum observables," *Phys. Rev. A, Gen. Phys.*, vol. 99, no. 1, Jan. 2019, Art. no. 012338.
[30] P. Czarnik, A. Arrasmith, P. J. Coles, and L. Cincio, "Error mitigation with Clifford quantum-circuit data," 2020, *arXiv:2005.10189*. [Online]. Available: http://arxiv.org/abs/2005.10189
[31] A. Strikis, D. Qin, Y. Chen, S. C. Benjamin, and Y. Li, "Learning-based quantum error mitigation," 2020, *arXiv:2005.07601*. [Online]. Available: http://arxiv.org/abs/2005.07601
[32] C. Kim, K. D. Park, and J.-K. Rhee, "Quantum error mitigation with artificial neural network," *IEEE Access*, vol. 8, pp. 188853–188860, 2020.
[33] A. Zlokapa and A. Gheorghiu, "A deep learning model for noise prediction on near-term quantum devices," 2020, *arXiv:2005.10811*. [Online]. Available: http://arxiv.org/abs/2005.10811
[34] M. S. Kaznady and D. F. James, "Numerical strategies for quantum tomography: Alternatives to full optimization," *Phys. Rev. A, Gen. Phys.*, vol. 79, no. 2, Feb. 2009, Art. no. 022109.
[35] D. McMahon, *Quantum Computing Explained*. Hoboken, NJ, USA: Wiley, 2007.
[36] M. Frey, D. Collins, and K. Gerlach, "Probing the qudit depolarizing channel," *J. Phys. A, Math. Theor.*, vol. 44, no. 20, Apr. 2011, Art. no. 205306.
[37] A. He, B. Nachman, W. A. de Jong, and C. W. Bauer, "Zero-noise extrapolation for quantum-gate error mitigation with identity insertions," *Phys. Rev. A, Gen. Phys.*, vol. 102, no. 1, Jul. 2020, Art. no. 012426.
[38] A. J. Scott and M. Grassl, "Symmetric informationally complete positive-operator-valued measures: A new computer study," *J. Math. Phys.*, vol. 51, no. 4, 2010, Art. no. 042203.
[39] J. ur Rehman and H. Shin, "Entanglement-free parameter estimation of generalized Pauli channels," *Quantum*, vol. 5, p. 490, Jul. 2021.

SYAHRI RAMADHANI received the B.S. degree in mathematics from Bandung Institute of Technology, Bandung, Indonesia, in 2016. She is currently pursuing the M.S. degree with the Department of Electronics and Information Convergence Engineering, Kyung Hee University. Her research interests include quantum information science, quantum computing, and quantum estimation theory.

JUNAID UR REHMAN received the B.E. degree in electrical engineering from the National University of Sciences and Technology (NUST), Pakistan, in 2013, and the Ph.D. degree in electronic engineering from Kyung Hee University, South Korea, in 2019. He is currently working as a Research Professor with the Department of Electronics and Information Convergence Engineering, Kyung Hee University. His research interests include general quantum channel models, quantum communications, and quantum process tomography techniques.

HYUNDONG SHIN (Fellow, IEEE) received the B.S. degree in electronics engineering from Kyung Hee University (KHU), South Korea, in 1999, and the M.S. and Ph.D. degrees in electrical engineering from Seoul National University, South Korea, in 2001 and 2004, respectively. During his postdoctoral research at the Massachusetts Institute of Technology (MIT), from 2004 to 2006, he was with the Wireless Communication and Network Sciences Laboratory under the supervision of Prof. Moe Win. In 2006, he joined KHU, where he is currently a Professor with the Department of Electronics and Information Convergence Engineering. His research interests include quantum information science, wireless communication, and nanonetworks. He received the IEEE Guglielmo Marconi Prize Paper Award, in 2008, and the IEEE William R. Bennett Prize Paper Award, in 2012. He was honored with the Knowledge Creation Award in the field of computer science from the Korean Ministry of Education, Science and Technology, in 2010. He served as the Publicity Co-Chair for the IEEE PIMRC, in 2018, and the Technical Program Co-Chair for the IEEE WCNC (PHY Track 2009) and the IEEE Globecom (Communication Theory Symposium 2012, and Cognitive Radio and Networks Symposium 2016). He was an Editor of IEEE TRANSACTIONS ON WIRELESS COMMUNICATIONS, from 2007 to 2012, and IEEE COMMUNICATIONS LETTERS, from 2013 to 2015.